journal of the mechanical behavior of biomedical materials 139 (2023) 105671

Contents lists available at ScienceDirect

Journal of the Mechanical Behavior of Biomedical Materials

journal homepage: www.elsevier.com/locate/jmbbm

Characterisation of native and decellularised porcine tendon under tension and compression: A closer look at glycosaminoglycan contribution to tendon mechanics

Jacqueline Solis-Cordova [a,b,*], Jennifer H. Edwards [a], Hazel L. Fermor [a], Philip Riches [c], Claire L. Brockett [b], Anthony Herbert [b]

[a] Institute of Medical and Biological Engineering, School of Biomedical Sciences, Faculty of Biological Sciences, University of Leeds, Leeds, United Kingdom
[b] Institute of Medical and Biological Engineering, School of Mechanical Engineering, Faculty of Engineering and Physical Sciences, University of Leeds, Leeds, United Kingdom
[c] Department of Biomedical Engineering, Faculty of Engineering, University of Strathclyde, Wolfson Centre, Glasgow, United Kingdom

ARTICLE INFO

Keywords:
Decellularisation
Tendon
Tissue scaffolds
Biomechanics
Glycosaminoglycans

ABSTRACT

Decellularised porcine superflexor tendon (pSFT) has been characterised as a suitable scaffold for anterior cruciate ligament replacement, with dimensions similar to hamstring tendon autograft. However, decellularisation of tissues may reduce or damage extracellular matrix components, leading to undesirable biomechanical changes at a whole tissue scale. Although the role of collagen in tendons is well established, the mechanical contribution of glycosaminoglycans (GAGs) is less evident and could be altered by the decellularisation process. In this study, the contribution of GAGs to the tensile and compressive mechanical properties of pSFT was determined and whether decellularisation affected these properties by reducing GAG content or functionality.

PSFTs were either enzymatically treated using chondroitinase ABC to remove GAGs or decellularised using previously established methods. Native, GAG-depleted and decellularised pSFT groups were then subjected to quantitative assays and biomechanical characterisation. In tension, specimens underwent stress relaxation and strength testing. In compression, specimens underwent confined compression testing.

The GAG-depleted group was found to have circa 86% reduction of GAG content compared to native and decellularised groups. There was no significant difference in GAG content between native (3.75 ± 0.58 μg/mg) and decellularised (3.40 ± 0.37 μg/mg) groups. Stress relaxation testing discovered the time-independent and time-dependent relaxation moduli of the decellularised group were reduced ≥50% compared to native and GAG-depleted groups. However, viscoelastic behaviour of native and GAG-depleted groups resulted similar. Strength testing discovered no differences between native and GAG-depleted group's properties, albeit a reduction ~20% for decellularised specimens' linear modulus and tensile strength compared to native tissue. In compression testing, the aggregate modulus was found to be circa 74% lower in the GAG-depleted group than the native and decellularised groups, while the zero-strain permeability was significantly higher in the GAG-depleted group (0.86 ± 0.65 mm^4/N) than the decellularised group (0.03 ± 0.04 mm^4/N).

The results indicate that GAGs may significantly contribute to the mechanical properties of pSFT in compression, but not in tension. Furthermore, the content and function of GAGs in pSFTs are unaffected by decellularisation and the mechanical properties of the tissue remain comparable to native tissue.

1. Introduction

Anterior cruciate ligament (ACL) ruptures affect 30 to 78 per 100,000 individuals annually (Gans et al., 2018). Following ACL rupture, a replacement graft is required to restore function and stability (Bliss, 2017). An optimal graft should match the anatomical dimensions and physiological demands of the native ACL, while providing a microenvironment which encourages development of neo-tissue

* Corresponding author. Institute of Medical and Biological Engineering, School of Mechanical Engineering, Faculty of Engineering and Physical Sciences University of Leeds, Leeds, LS2 9JT, UK.
E-mail address: bsbjsc@leeds.ac.uk (J. Solis-Cordova).

https://doi.org/10.1016/j.jmbbm.2023.105671
Received 29 September 2022; Received in revised form 17 November 2022; Accepted 7 January 2023
Available online 11 January 2023

(Rahouadj et al., 2018). Currently, surgeons rely on autografts and allografts for this procedure (Macaulay et al., 2012), which suffer biological and mechanical limitations (Woods and Gratzer, 2005; Vyas et al., 2012; Janssen and Scheffler, 2014; Villa Albers et al., 2017; Jamil et al., 2017). However, decellularised porcine tendon provides an off-the-shelf graft option eliminating donor site morbidities, and offering plentiful supply via the food chain.

Decellularised tendon is produced by removing the immunogenic components of the porcine source tissue, such as cellular material and markers, nucleic acids and antigens (α-Gal epitopes) (Choi et al., 2012). This reduces foreign body reaction, inflammation and adverse immune response when implanted into a host (Fishman et al., 2013). A biocompatible extracellular matrix (ECM) scaffold is obtained, providing mechanical function in addition to biochemical and biological cues (Gilpin and Yang, 2017; Sackett et al., 2018). This leads to matrix health, renewal and development of new functional tissue by host cells (Edwards et al., 2021).

However, the decellularisation process could adversely affect the structural and mechanical properties of biological tissues (Crapo et al., 2011; Gilbert et al., 2006). The decellularisation protocol used within our group was initially developed for porcine meniscus (Stapleton et al., 2008), with low concentration ionic detergent (SDS) washes. The basis for this process has been patented (PCT/GB02/02341) and subsequently licenced to external organisations. In both meniscus and osteochondral plugs subjected to the decellularisation process, a reduction in GAG content and mechanical properties was observed (Stapleton et al., 2008; Fermor et al., 2015; Abdelgaied et al., 2015). This heightens the importance of determining the contribution of this matrix component to the mechanical properties of porcine tendon, to investigate if decellularisation could affect GAG related mechanical function.

Decellularised porcine superflexor tendon (pSFT) has been extensively studied as a potential biological scaffold for use in ACL replacement (Herbert et al., 2015, 2017; Jones et al., 2017; Edwards et al., 2017, 2019, 2021; Whitaker et al., 2019). Although the decellularisation process does not alter collagen within the ECM, glycosaminoglycans (GAGs) appear to be removed (Jones et al., 2017) which may translate to minor reductions in the tensile mechanical properties of the tendon (Herbert et al., 2015; Edwards et al., 2019). It is not clear however, if the reductions in mechanical properties are linked directly with GAG loss or if they are a consequence of some other decellularisation-associated mechanism.

Previous biomechanical studies on pSFT have focused on its properties under tension, as it is the principal mode of load transmission. However, tendon may also experience lateral compressive loads (Vogel and Koob, 1989), as they function in complex *in vivo* loading environments (Fang and Lake, 2015), subject to multiaxial states of stress (Docking et al., 2013). Furthermore, interference screws are the most commonly used direct mechanical fixation method in ACL replacement (Speziali et al., 2014), which act by compressing the graft against the host bone environment (Harvey et al., 2005). A potential graft should offer a degree of compressive resistance normal to the main axis of collagen fibre alignment to ensure adequate fixation. Therefore, a complete mechanical assessment of a decellularised biological scaffold for ACL replacement should determine both tensile and compressive properties to ensure the decellularisation process has not overly affected these. Limited studies on compressive properties of tendon exist in the literature (Koob et al., 1992; Lee et al., 2000; Williams et al., 2008; Fang et al., 2014; Böl et al., 2015). To the author's knowledge, there are no reported compression experiments on decellularised tendon.

In this study, it was hypothesised that the quantity of GAGs in pSFT would be reduced following decellularisation, in agreement with previously reported findings on this and other tissues. The GAGs that remained post-decellularisation would retain all, if not, partial mechanical function. Given the relatively low initial GAG content of pSFT, it was expected that the tissue's tensile mechanical properties following decellularisation would not significantly differ from unprocessed, native pSFT. However, despite the low initial GAG content, a reduction post-decellularisation was anticipated to adversely impact pSFT compressive mechanical properties. This study therefore aimed to determine the contribution of GAGs to the tensile and compressive mechanical properties of native pSFT and if decellularisation reduced GAG content to the extent of affecting these properties.

2. Material and methods

2.1. Experimental design

Porcine superflexor tendon (pSFT) has previously been studied in this group, establishing protocols for decellularisation and biomechanical testing (Herbert et al., 2015, 2017; Jones et al., 2017; Edwards et al., 2017, 2019; Whitaker et al., 2019). Three sample groups were analysed ($n = 6$ for each), including native, GAG-depleted and decellularised pSFT. Biomechanical characterisation was conducted by subjecting specimens to tensile and compressive loads. In tension, specimens underwent stress relaxation and strength testing coaxially to the collagen fibres, representing the tendon's main axis of loading. In compression, specimens underwent confined loading with primary collagen fibres transverse to the compressive test axis.

2.2. Tissue sourcing

The hind legs of Large White pigs (age ~4 months, mixed sex, 85.24 ± 2.34 kg) were obtained from abattoirs (Yorkshire Farmers, Meadow Quality Ltd, Scotlean Ltd; United Kingdom) within 24 h of slaughter. The pSFT, which extends from the toe (T) to the ankle (A), was located and removed (Fig. 1). The dissection of the pSFT was adapted from previous studies (Jones et al., 2017). The pSFT was located inferior to the superficial flexor tendon (*) after removal of the skin and subcutaneous tissue (Fig. 1a) of the foot region using a scalpel and then creating an incision longitudinally towards (A). Connective tissue was removed carefully to prevent damaging the bulk tissue (Fig. 1b). An accessory ligament (Fig. 1c) of the deep digital flexor muscle is located approximately halfway along the pSFT. A cut was made close to the pSFT releasing it from the accessory ligament. The pSFT was isolated by making an incision at the myotendinous junction, releasing from (A) and at the interdigital space, releasing from (T) (Fig. 1d and e).The tendons (Fig. 1f) were stored at −20 °C wrapped in filter paper dampened with phosphate buffered saline (PBS; Oxoid) until required.

2.3. Biological methods

2.3.1. Decellularisation of pSFTs

The decellularisation protocol was adapted from a previous study (Jones et al., 2017). pSFTs were subjected to two freeze–thaw cycles between −20 °C and room temperature (RT), both times with pSFTs immersed in hypotonic buffer plus proteinase inhibitors (10 mM Tris [Sigma Aldrich]; 2.7 mM disodium ethylene-diamine-tetra acetic acid [EDTA; Thermo Fisher Scientific]; 10 KIU/mL aprotinin [Nordic Pharma], pH 8.0). Specimens were then washed in acetone (WVR International) three times for 1 h (RT), then washed five times in PBS plus aprotinin (10 KIU/mL) at RT. pSFTs were disinfected in a combination of penicillin-streptomycin (Sigma) and amphotericin B (Sigma) diluted (1:50) in PBS for 1 h. All subsequent steps in the process were conducted on tendons in individual 150 mL sterile pots containing 100 mL of each solution at 42 °C with agitation, unless otherwise stated. Tendons were washed in hypotonic buffer for 24 h and then hypotonic buffer plus 0.1% (w/v) sodium dodecyl sulfate (SDS; Sigma) for 24 h. These washes were repeated twice. pSFTs were washed for 3 × 30 min in PBS plus aprotinin, then for 1 × 72 h, and then in PBS with no additives for 3 × 30 min. Specimens were then treated with nuclease (1 U/mL benzonase [Merck] in 60 mL 50 mM Tris plus 1 mM $MgCl_2$ [Thermo Fisher Scientific] at pH 7.6) for 2 h, three times. pSFTs were washed three times in PBS plus 2.7

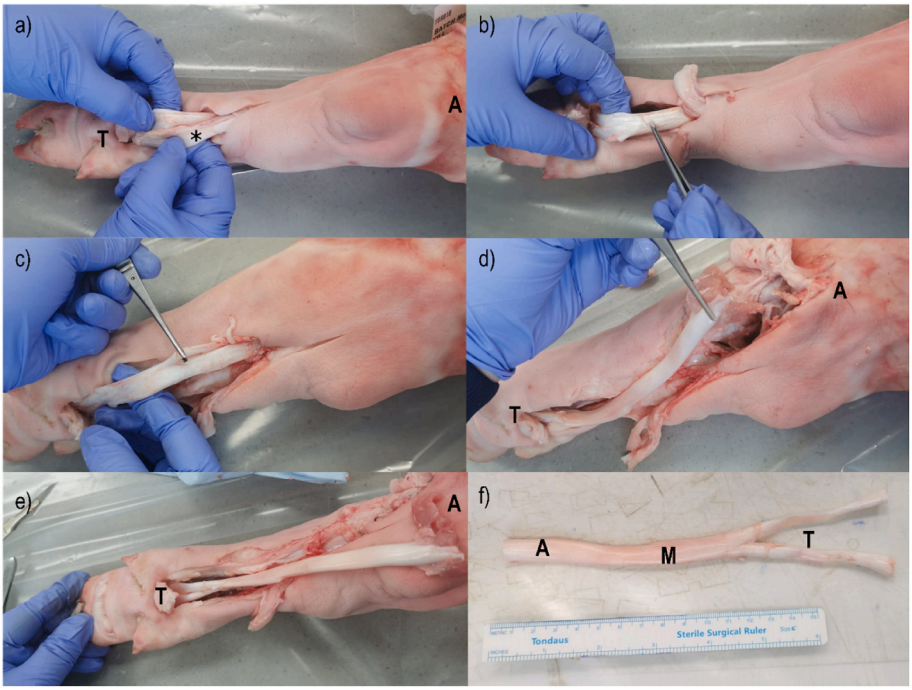

Fig. 1. Dissection of pSFT from porcine hind leg. a) pSFT inferior to deep digital flexor tendon (*), extending from toe (T) to ankle (A) region; b) removal of superficial digital flexor tendon and connective sheath tissue; c) accessory ligament of deep digital flexor muscle; d) incision at the myotendinous junction releasing SFT from ankle attachment site (A); e) incision at interdigital space releasing SFT from toe attachment site (T); and f) whole SFT with toe (T), middle (M) and ankle (A) portions.

mM EDTA before an 18–20h wash in hypertonic buffer (50 mM Tris; 1.5 M NaCl [Sigma]; pH 7.6). After 3 × 30 min PBS washes, pSFTs were sterilised using peracetic acid (0.1% v/v, pH 6; Sigma) for 3 h pSFTs were washed in PBS for 3 × 30 min, then for 1 × 48 h, 1 × 72h, then for 1 × 1 week and finally stored at −20° C.

2.3.2. GAG removal and assessment

2.3.2.1. Chondroitinase ABC treatment. Digestion with ChABC (Sigma) was adapted from a previous study (Henninger et al., 2010). Briefly, pSFTs (n = 6 treated; n = 6 control) were placed in 150 mL sterile pots. Specimens were equilibrated for 1 h in 60 mL control buffer at 37°C, with gentle agitation using an orbital shaker (80 rpm). Control buffer consisted of full-strength Ringer's solution containing 20 mM Tris (pH 8.0), 0.1 M sodium acetate and protease inhibitor (10 KIU/mL aprotonin; Nordic Pharma). Specimens were then treated for 72 h in either control or treatment buffer in the same temperature and agitation conditions. Treatment buffer was control buffer with the addition of 0.1 U/mL ChABC.

2.3.2.2. GAG quantification. GAG content of native, GAG-depleted and decellularised pSFTs (n = 6 in all cases) was determined using the dimethylene blue assay. Specimens were macerated and freeze-dried. Specimens were then digested in papain (800 KU/mL; Acros Organics) for 36 h at 60°C, vortexed midway through the incubation period. Standard and test samples (40 μL) were added to 96-well plates with 250 μL 1,9-dimethylene blue solution (DMB). Absorbance was read at 525 nm after 2 min incubation. The sulfated sugar content of test samples was calculated by interpolation from the standard curve generate from known concentrations of chondroitin sulfate B (μg/mL; Sigma).

2.3.3. Histological evaluation

Transverse and longitudinal samples were taken from each tendon and fixed in 10% (v/v) neutral buffered formalin (NBF; Atom Scientific) for 24 h for histochemical staining. The samples were processed automatically (Leica 11020 Tissue processor) and embedded in paraffin wax (Leica EG1150 C Tissue embedding system).

To validate the decellularisation process, 8 μm sections were taken from the surface through to the central region of native and decellularised specimen blocks and stained with haematoxylin (Atom Scientific) and eosin (Merck Millipore) (H&E), 4', 6-diamidino-2-phenylindole dihydrochloride (DAPI; Sigma).

For qualitative assessment of GAG content, sections (8 μm) were taken from native, GAG-depleted and decellularised specimen blocks and stained with Safranin O (Raymond Lamb)/Fast green (Sigma) (SafO).

All sections were viewed using an upright microscope (AXIO Imager. M2, Zeiss). Sections stained with H&E and SafO were viewed using Köhler (bright field) illumination, while DAPI stained sections were viewed using fluorescent illuminators. Images were captured digitally using the associated digital camera (AXIOCAM MRc5, Zeiss).

2.4. Biomechanical methods

2.4.1. In tension

2.4.1.1. Specimen preparation. Native, GAG-depleted and decellularised pSFTs (n = 6 in all cases) were immersed in dry ice and snap frozen. They were then cut into dumbbell shapes with cross-sectional areas of approximately 3.5 × 5 mm (natural thickness) and a gauge length of 30 mm. All specimens were wrapped in PBS soaked filter paper and stored at −20 °C until required for testing.

On test day, specimens were thawed at room temperature for 2 h prior to tensile characterisation. Each specimen was equilibrated in PBS-soaked filter paper at room temperature for 1 h. Dimensional measurements were taken immediately prior to mechanical testing. Specimens were mounted using bespoke cryogrips (Herbert et al., 2015) to an Instron 3365 material testing machine (Instron, Bucks, UK).

2.4.1.2. Stress relaxation testing. Stress relaxation testing was adapted from previous studies (Herbert et al., 2015, 2017). The Instron 3365 was equipped with a 500 N load cell. Specimens were tensioned to a pre-load of 0.25 N, then ramp loaded at a rate of 30 mm min^{-1} until a stress of 5 MPa was reached. This stress has previously been reported physiologically relevant based on studies of *in vivo* tensile loads of the ACL (Herbert et al., 2015). The specimens were then held at the corresponding strain

reached at the end of the ramp for a period of 200 s allowing stress relaxation to occur. Data was recorded at a frequency of 10 Hz.

The relaxation modulus, *E(t)*, was calculated by dividing engineering stress by the engineering strain in the following manner:

$$E(t) = \sigma(t)/\varepsilon_0$$

where $\sigma(t)$ and ε_0 are the stress relaxation data and the fixed held strain respectively.

This was fitted ($r^2 > 0.96$) to a modified second order Maxwell-Weichert model (Jimenez Rios et al., 2007), using the non-linear least squares method:

$$E(t) = E_0 + \frac{1}{t_0}\left[E_1\tau_1 e^{-\frac{t}{\tau_1}}\left(e^{-\frac{t_0}{\tau_1}} - 1\right) + E_2\tau_2 e^{-\frac{t}{\tau_2}}\left(e^{-\frac{t_0}{\tau_2}} - 1\right)\right]$$

where E_0 represents a time-independent elastic modulus, E_1 and E_2 represent time-dependent elastic moduli, τ_1, τ_2 represents the respective relaxation times.

2.4.1.3. Strength testing. Strength testing was adapted from previous studies (Herbert et al., 2015; Jones et al., 2017; Edwards et al., 2017). The Instron 3365 was equipped with a 5 kN load cell. A pre-load of 0.25 N was applied to ensure tautness. Tensile testing consisted of 12x pre-conditioning cycles between 0% and 5% strain at a strain rate of 50% min^{-1}, followed by an extension ramp to failure at a rate of 100% min^{-1}. Data was recorded at a frequency of 10 Hz. Stress was calculated by dividing the force recorded by the load cell by the cross-sectional area of the pSFT, whereas strain was calculated by dividing the crosshead displacement by the gauge length of each specimen. Stress and strain data were used to determine the ultimate tensile strength (*UTS*) and strain at failure (ε_{fail}). A bespoke bi-linear model was fitted to stress-strain data using a custom written Matlab script (Herbert et al., 2016). This provided the quantitative values for toe and linear region moduli (E_{toe} and E_{linear} respectively).

2.4.2. In compression

2.4.2.1. Specimen preparation. A cylindrical plug specimen (Fig. 2a) was obtained from the mid-substance of native, GAG-depleted and decellularised pSFTs (n = 6 in all cases) using a 6 mm diameter biopsy punch (Sigma-Aldrich 6 mm Harris Uni-Core). The punch was positioned normal to the lateral anatomical surface of the tendon. This produced cylindrical specimens with collagen fibres orientated normal to the test axis, i.e. transverse plane. Specimen height was the natural tendon thickness, measured at two points using Vernier callipers and an average calculated. Samples were stored at −20 °C in bijous with filter paper dampened with PBS until required for testing.

2.4.2.2. Confined compression testing. Specimens were mounted on an Instron 3365 material testing machine using a custom-designed apparatus. Briefly, it consisted of a confining cylindrical chamber comprised of upper and lower sections. The lower section held the porous platen (25.4 mm diameter; Porous 316L SS disc Media Grade 5; Mott Corporation) which allowed fluid exudation in a downward direction. The upper chamber had a simple centred hole (6 mm diameter). The specimen was placed inside the central 6 mm hole with the bottom surface of the specimen in contact with the porous platen (Fig. 2b). A stainless steel plunger of the same diameter as the central hole was mounted to the crosshead of the Instron, which would provide compression to the sample. A spacer allowed mounting of the chamber to the Instron. All elements of the set-up were immersed in a bath containing PBS at 37 °C.

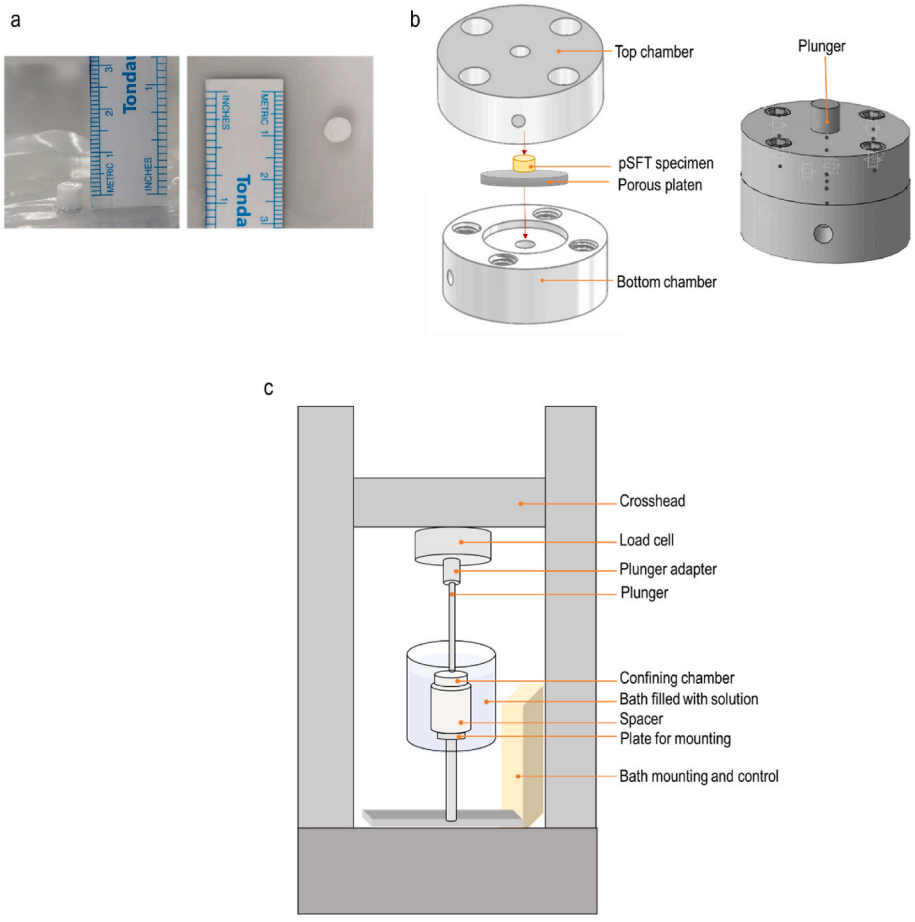

Fig. 2. Sample preparation and confined compression testing of pSFT. The prepared specimens (a) as seen perpendicularly showing the fascicular mid-substance flanked by peritenon at either end (left) and transversely to the middle region of the anatomical tendon surface or peritenon (right). Confining delrin chamber with cylindrical pSFT specimen confined within (b), showing relative position of specimen within top and bottom chamber on the left; confining chamber held together by M4 bolts with pSFT specimen inside on the right. Elements mounted onto Instron 3365 material testing machine (c), with confining chamber equilibrating inside bath, ready for compressive loading by action of the plunger.

Specimen set-up is represented in Fig. 2c.

The Instron 3365 was equipped with a 5 kN load cell. Specimens were allowed to equilibrate within confined conditions while submerged in the temperature-controlled PBS bath for 15 min. To ensure full specimen contact with the plunger and to set the starting position, the plunger was lowered until a load of 2.5 N was recorded. This load was held for 60 s, before being reduced to 0.25 N for a holding period of 300 s. Instron displacement and load channels were then zeroed. Specimens were then subjected to a displacement ramp at a rate of 1% s^{-1} until a compressive strain of 10% was reached and held for a period of 600 s. Data was recorded at a frequency of 10 Hz. This level of applied strain was considered appropriate given similar compression studies conducted on cartilage (Chan et al., 2016), as there is limited compressive characterisation conducted on tendon.

Peak stress was taken as the stress value occurring at 10% strain, while equilibrium stress was taken as an average of stress of the final 30 s of the hold period. Biphasic theory parameters aggregate modulus (H_A), zero-strain permeability (k_0) and strain-dependent permeability coefficient (M) (in which permeability, $k = k_0 \exp(M\varepsilon)$ where ε is the strain) were inversely fitted to the relaxation and hold phase data employing FEBio (v 2.8) (Maas et al., 2012) and custom Matlab algorithms using a Nelder-Mead scheme (Busby et al., 2013).

2.5. Statistical analysis

Prior to analysis, data was checked for normal distribution using the Kolmogorov-Smirnov normality test. Statistical variances between groups were determined using a one-way analysis of variance (ANOVA). Tukey's significant difference test was used for post-hoc evaluation. A p-value of <0.05 was considered to be significant.

3. Results

3.1. Biological characterisation

3.1.1. Validation of decellularisation process

Sections of native pSFT stained with H&E (Fig. 3a) and DAPI (Fig. 3b) revealed the presence of cells throughout tissue matrix. Blood vessels were apparent where cell density increased (arrows). Sections of decellularised pSFT stained with H&E (Fig. 3c) and DAPI (Fig. 3d) showed absence of cell nuclei, cell debris and nucleic acid. Matrix architecture appeared similar to native tissue, with a slightly more open matrix.

3.1.2. GAG content of native, GAG-depleted and decellularised pSFTs

The total sulfated GAG content of the native pSFT group was found to be 3.75 ± 0.58 μg/mg (mean ± 95% CI). After treatment with low concentration ChABC, GAG content was significantly reduced to 0.51 ± 0.20 μg/mg ($p < 0.0001$). Enzymatic treatment removed circa 86% of GAGs in pSFT extracellular matrix (Fig. 4). Following decellularisation, GAG content was not significantly different from native pSFT, with 3.40 ± 0.37 μg/mg ($p = 0.335$).

Safranin O/Fast Green stained sections of native (Fig. 5a and b) pSFT

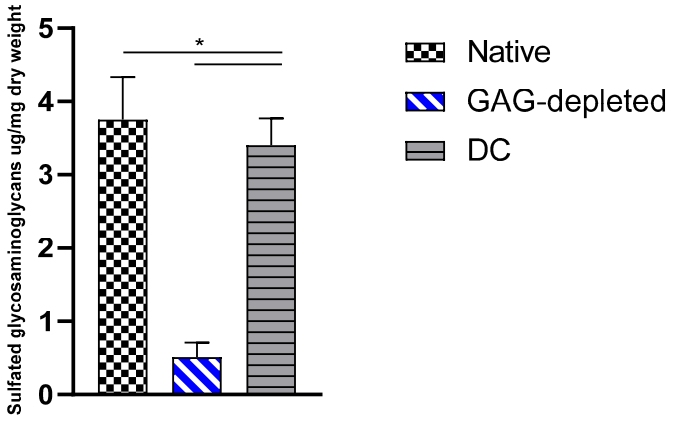

Fig. 4. Total sulfated GAG content of native, GAG-depleted and decellularised (DC) pSFT. No significant difference between native and DC specimens, both significantly higher than GAG-depleted specimens. Data is presented as mean (n = 6) ± 95% CI. Data was analysed using one-way ANOVA followed by Tukey's post hoc test. * indicate significant difference between groups.

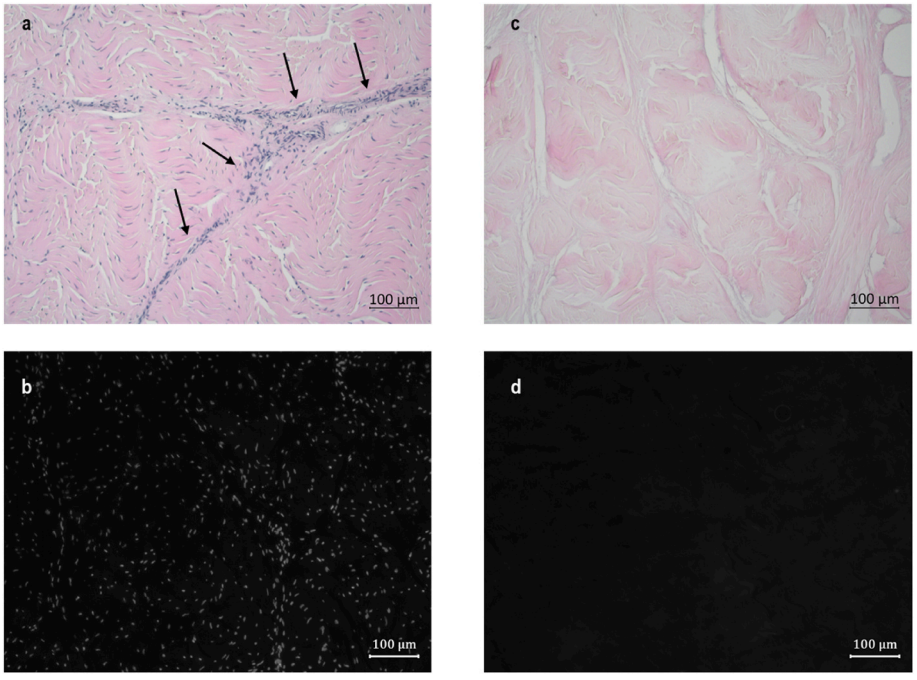

Fig. 3. Representative micrographs of sections of pSFT stained with haematoxylin and eosin (H&E) (a, c) and 4′, 6-diamidino-2-phenylindole dihydrochloride (DAPI) (b, d). Transverse sections of native (a, b) and decellularised (c, d) pSFT, show characteristic blue/purple cell nuclei in H&E stained native (a) sections and no cellular nuclei or debris post-decellularisation (c). Fluorescent nucleic acid stained with DAPI in native (b) sections, with no fluorescence in decellularised (d) pSFT. Images were taken at 100 x magnification (scale bar 100 μm).

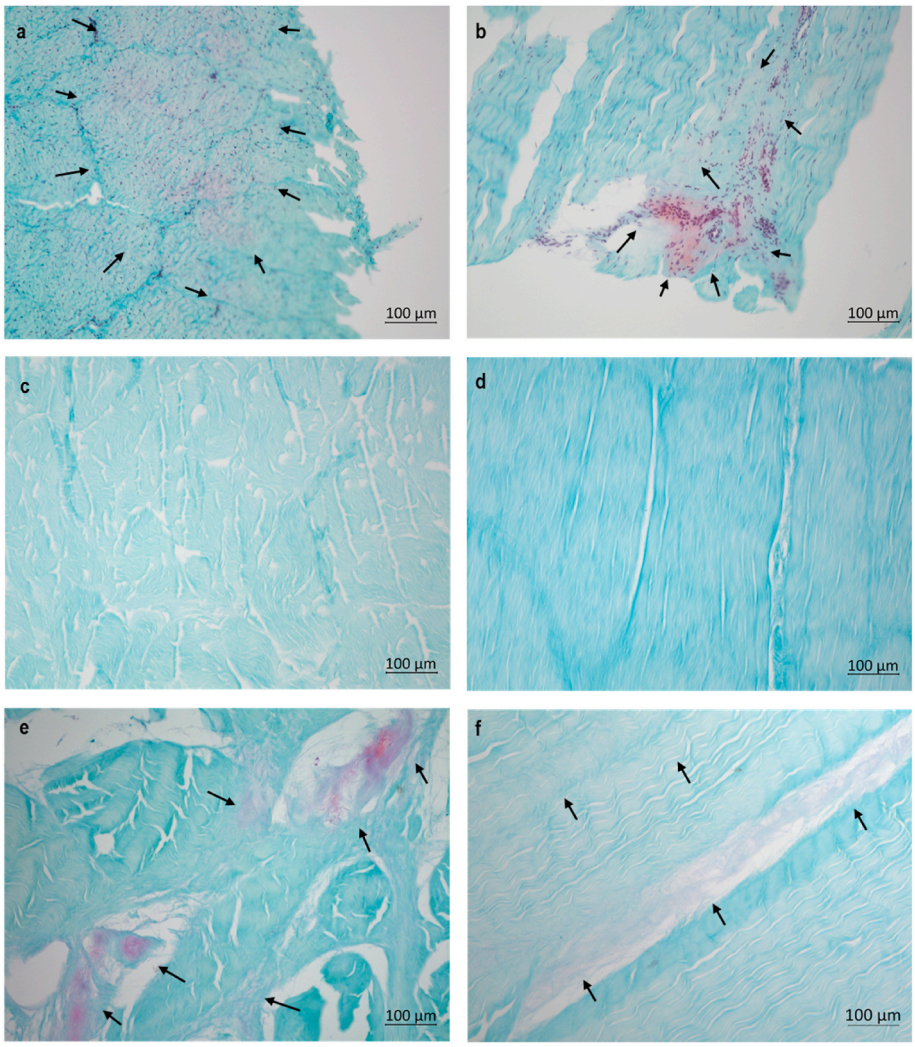

Fig. 5. Representative micrographs of sections of pSFT stained with safranin O and Fast Green. Transverse (a, c, e) and longitudinal (b, d, f) sections of native (a, b), GAG-depleted (c, d) and decellularised (e, f) pSFT show presence of GAGs in native and decellularised sections but not in GAG-depleted sections. Images were taken at 100 x magnification (scale bar 100 μm).

showed GAGs sparsely distributed throughout the fascicular matrix in transverse sections (Fig. 5a), while visibly aligned between the collagen in longitudinal sections (Fig. 5b). GAG-depleted sections (Fig. 5c and d) showed no GAGs. The lack of cell nuclei observed was attributed to the role of GAGs in cell to cell and cell to extracellular matrix adhesion (Wight et al., 1992; Shi et al., 2021; Casale and Crane, 2022). In cleaving GAGs and associated proteoglycans, these mechanisms were disrupted, leading to loss of cellular material during enzymatic depletion and subsequent fixing, processing and staining processes. Decellularised sections (Fig. 5e and f) showed GAGs distributed throughout the matrix, distributed across a more open structure (Fig. 5e) compared to native sections.

Table 1
Stress relaxation parameters. Data were compared using one-way ANOVA followed by Tukey's post hoc test. Groups in each column that do not share the same superscript are significantly different. Data are presented as means (n = 6) ± 95% CI.

	E_0 (MPa)	E_1 (MPa)	E_2 (MPa)	τ_1 (s)	τ_2 (s)
Native	207.90 ± 45.60^{a}	14.94 ± 7.24^{a}	6.52 ± 3.08^{a,b}	0.84 ± 0.32	4.10 ± 3.50
GAG-depleted	209.03 ± 37.65^{a}	24.03 ± 3.23^{b}	10.45 ± 6.67^{b}	0.92 ± 0.71	7.64 ± 7.18
Decellularised	84.04 ± 19.84^{b}	6.98 ± 2.21^{c}	1.97 ± 2.40^{a}	0.96 ± 0.43	7.97 ± 3.12

3.2. Biomechanical characterisation

3.2.1. Tensile testing

Stress relaxation parameters are summarised in Table 1. There was no significant difference in the time-independent relaxation moduli (E_0) between native and GAG-depleted groups. However, there was significant reduction in the decellularised group when compared to remaining groups ($p < 0.0001$). The time-dependent relaxation moduli, E_1, of native specimens was significantly reduced compared to GAG-depleted ($p = 0.012$), but higher than decellularised ($p = 0.028$). The time-dependent relaxation moduli, E_2, was significantly reduced for decellularised specimens compared to GAG-depleted ($p = 0.013$), but not different from native pSFT.

When subjected to strength testing, mid-substance failure of all specimens was achieved. There were no significant differences between native and GAG-depleted group's properties (Table 2). There was a significant reduction in E_{linear} of the decellularised specimens compared to both native ($p = 0.044$) and GAG-depleted ($p = 0.029$) groups. Similarly, UTS was significantly reduced for decellularised specimens compared to GAG-depleted ($p = 0.012$), but not different from native

Table 2
Strength testing parameters determined by uniaxial tensile testing. Data were compared using one-way ANOVA followed by Tukey's post hoc test. Groups in each column that do not share the same superscript are significantly different. Data are presented as means (n = 6) ± 95% CI.

	E_{toe} (MPa)	E_{linear} (MPa)	UTS (MPa)	ε_{Fail} (mm/mm)
Native	78.20 ± 18.29	585.77 ± 111.18[a]	67.40 ± 9.06[a,b]	0.18 ± 0.02
GAG-depleted	110.35 ± 86.41	611.03 ± 86.08[a]	79.37 ± 15.53[a]	0.17 ± 0.02
Decellularised	38.94 ± 17.78	441.06 ± 82.86[b]	55.53 ± 11.84[b]	0.20 ± 0.03

pSFT.

3.2.2. Confined compression testing

No significant differences were found between all groups for the heights of specimen plugs ($p > 0.05$). The peak stress of native specimens was significantly higher than GAG-depleted ($p < 0.0001$) and decellularised specimens ($p = 0.002$). GAG-depleted specimens achieved circa 11% of native peak stress (Fig. 6a). The equilibrium stress of native specimens was not significantly different from GAG-depleted or decellularised specimens (Fig. 6b). However, GAG-depleted specimens did have a significantly reduced equilibrium stress compared to decellularised specimens ($p = 0.003$).

The aggregate modulus of native specimens was significantly greater than the GAG depleted group ($p = 0.018$). The aggregate modulus decreased with reduced GAG content (Fig. 7), with a ~74% reduction compared to native pSFTs. Decellularised specimens had a similar aggregate modulus to native specimens, and likewise was significantly greater compared to GAG-depleted pSFTs ($p = 0.011$).

The zero-strain permeability (k_0) of native specimens was not significantly different from GAG-depleted specimens ($p = 0.177$). However, contrary to the aggregate modulus, permeability of GAG-depleted specimens resulted significantly higher than decellularised pSFTs ($p = 0.009$). The decellularised group showed a ~93% reduction compared to native pSFTs (Fig. 8a). The nonlinear permeability coefficient (M) significantly decreased in both GAG-depleted ($p = 0.012$) and decellularised groups ($p = 0.001$) compared to native specimens (15.3 ± 2.7) (Fig. 8b).

4. Discussion

This study aimed to determine the contribution of GAGs to the tensile and compressive mechanical properties of pSFT. The investigation also assessed the effect of decellularisation on pSFT biomechanics.

Treatment of pSFT with ChABC removed circa 86% of GAGs (Fig. 4).

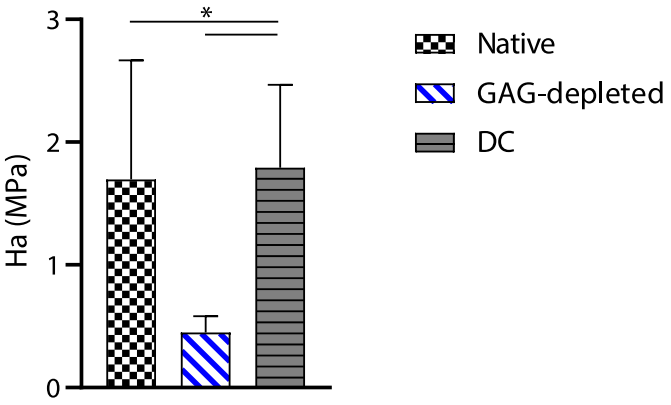

Fig. 7. Aggregate modulus of native, GAG-depleted and decellularised (DC) pSFTs. Significant reduction in aggregate modulus of GAG-depleted group compared to both native and DC pSFTs. Data is presented as mean (n = 6) ± 95% CI. Data was analysed using one-way ANOVA followed by Tukey's post hoc test. * indicate significant difference between groups.

This reduction is expected to be due to cleaving chondroitin sulfate A, C, dermatan sulfate and hyaluronic acid chains (Ernst et al., 1995). The remaining 14% of GAGs were therefore likely keratan and heparan sulfate chains (Screen et al., 2005, 2006). Histological staining using safranin O/fast green revealed no GAGs were present post ChABC treatment for the GAG-depleted group (Fig. 5c and d), validating GAG removal effectiveness. Decellularised pSFT retained similar GAG levels to native tendon (Fig. 4). Both groups showed characteristic red/pink GAGs distributed throughout native (Fig. 5a and b) and decellularised (Fig. 5e and f) fascicular matrix. Quantitative and qualitative assessments demonstrated the decellularisation process does not reduce GAG content in pSFT. This conflicts with a previous study conducted on native and decellularised pSFT showing a 75% reduction in GAGs post-decellularisation (Jones et al., 2017). However, initial GAG content of native pSFT was quantified at circa 6.85 μg/mg, an increase of ~83% with respect to this study. GAG content of both native and decellularised pSFT in Jones et al. may be indicative of variability in the yield of porcine tissue, compositional variations given the time of year it was procured due to changing dietary patterns, or an inherent variability of the tissue itself (Kim et al., 2019), such as animal maturity, weight and activity level. Furthermore, the region of the tendon selected for GAG quantification of native and decellularised groups could have influenced the outcome (Feitosa et al., 2006), not representative of GAG reduction caused by the decellularisation process itself. Here, we have demonstrated for the first time that GAG content is not reduced during the decellularisation process.

There was no significant difference in the time independent

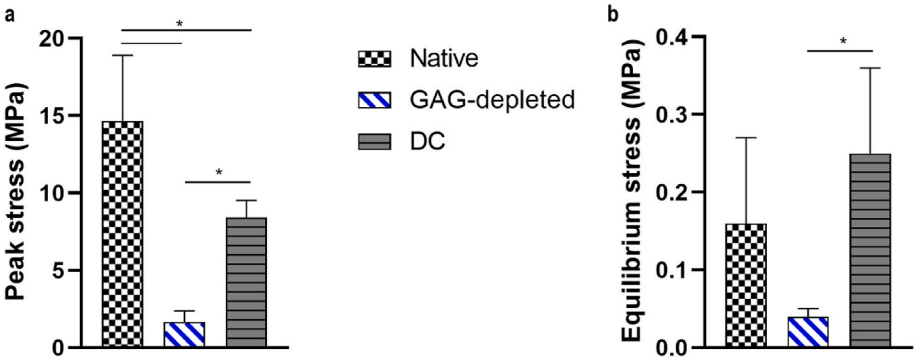

Fig. 6. Peak and equilibrium stress of native, GAG-depleted and decellularised (DC) pSFTs. Significantly reduced peak stress (a) of GAG-depleted specimens compared to native and DC pSFTs. Significant reduction in equilibrium stress (b) of GAG-depleted group compared to DC pSFTs. Data is presented as mean (n = 6) ± 95% CI. Data was analysed using one-way ANOVA followed by Tukey's post hoc test. * indicate significant difference between groups.

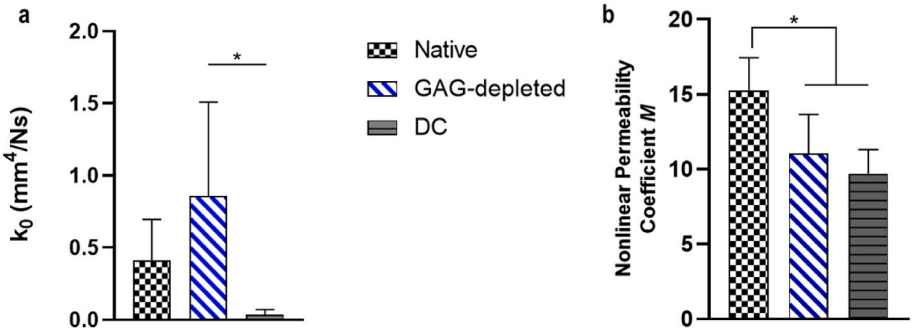

Fig. 8. Zero-strain permeability and strain-dependent permeability coefficient of native, GAG-depleted and decellularised (DC) pSFTs. Significant increase in permeability (a) of GAG-depleted pSFTs compared to DC. Significant decrease in permeability coefficient (b) of GAG-depleted and DC specimens compared to native. Data is presented as mean (n = 6) ± 95% CI. Data was analysed using one-way ANOVA followed by Tukey's post hoc test. * indicate significant difference between groups.

behaviour (E_0) of native and GAG-depleted pSFT in the stress relaxation testing. For the time-dependent moduli, a significant increase was observed only for E_1 in GAG-depleted specimens, while no other differences were found with respect to native tissue. This could support the hypothesis that GAGs do not play a significant role in the tensile viscoelastic behaviour of tendon, attributed to the structural integrity and organisation of the collagen, which is sufficient to compensate for the contribution of GAGs under tension. Such findings align with a study conducted on human medial collateral ligament (Lujan et al., 2009). There was a significant reduction in the time-independent relaxation modulus (E_0) and time-dependent (E_1) moduli of the decellularised pSFT group compared to both native and GAG-depleted groups. Only E_2 was not statistically different from native tissue. It has been proposed that collagen fibrils mainly contribute to the short-term viscoelastic response of collagenous tissue (Gautieri et al., 2013). This could be indicative of an effect the decellularisation process has on this component. Moreover, the interfascicular matrix (IFM) has been related to mediating the viscoelasticity of tendons (Screen, 2008). It is possible the IFM may have been affected during the decellularisation process with ensuing changes in decellularised pSFT viscoelastic behaviour. A disruption to the IFM in combination with cell removal may have caused a spatial rearrangement of intrafascicular collagen fibrils, resulting in the significantly greater and faster relaxation rate. However, there was considerable variance across these parameters in all groups. Certain parameters may be more sensitive to variation given the experimental conditions. The variance observed (long-term relaxation parameters) may be attributed to the duration of the stress relaxation experiment. In the latter stages of testing, the temperature of the grips may have caused further incremental freezing of a specimen, resulting in an outlier for a given parameter.

There were no observable differences between the tensile stress-strain profiles of native and GAG-depleted pSFT and accordingly, the classical material properties (E_{linear}, UTS, ε_{fail}) were not significantly different between these groups. This suggests that GAG removal does not contribute to a reduction in pSFT material properties in tension. These results align with a study conducted on human medial collateral ligament (Lujan et al., 2007), and studies conducted at a sub-tendon scale (Fessel and Snedeker, 2011; Svensson et al., 2011; Rigozzi et al., 2013). It can therefore be suggested that collagen is the principal ECM component contributing to the tensile mechanical properties of tendon, likely supported in some minor capacity by non-collagenous matrix components other than PG-GAGs. However, there was variance observed in the GAG-depleted group, hypothesised to be a consequence of GAG removal on the structural integrity of the tissue. This may have caused the tissue to become more compliant and sensitive to initial preloading conditions applied during testing. Decellularised specimens showed a significant reduction in E_{linear} compared to both native and GAG-depleted groups, while UTS was only significantly reduced with respect to GAG-depleted pSFT, but not significantly different from native tissue. Decellularisation did not affect GAG content in pSFT, further suggesting their role is not significant under tensile quasi-static conditions. This may indicate collagen density and micro-organisation (Shadwick, 1990), as well as inter- and intra-molecular bonds of collagen (Viidik, 1966) could be affected by the decellularisation process, possibly as a consequence of exposure to SDS (Gilpin and Yang, 2017). This could affect collagen crimp and extension, as smaller crimp angles may lead to earlier fibre failure (Wilmink et al., 1992). This also relates to the non-statistical reduction in the toe modulus of decellularised specimens. Strength testing parameters obtained here align with previous studies conducted on pSFT (Herbert et al., 2015; Jones et al., 2017; Edwards et al., 2019). Nevertheless, most material properties were within a comparable range to native tissue, suitable to act as a potential graft.

The aggregate modulus is a flow-independent measure of tissue stiffness, i.e. the intrinsic stiffness of the solid matrix. As aggregate modulus increases, a tissue is more capable of resisting deformation under load (Mansour, 2003). The aggregate modulus of both native and decellularised pSFT was significantly greater than GAG-depleted specimens, suggesting a strong contribution of GAGs in resisting compressive forces. This could be explained through the water-binding function of GAGs (Ryan et al., 2015). Upon removal, rapid fluid exudation occurs, translating to a diminished capability of supporting compressive loads. Given the enzymatic action mechanism for GAG depletion, it could be hypothesised that dermatan and chondroitin sulfate are the principal GAGs involved. Chondroitin sulfate has been found to resist compressional forces in cartilage matrix (Baeurle et al., 2009), concurring with this hypothesis. The similarity between the aggregate modulus of native and decellularised groups may indicate the decellularisation process does not adversely affect the mechanical function of the GAGs. The compressive peak and equilibrium stresses also demonstrated significant reductions relative to GAG content, possibly relating to its key role in bearing compressive forces. The reduction in compressive peak stress is in agreement with previous findings involving porcine ligament (Henninger et al., 2010). Decellularised specimens also showed a significant reduction in compressive peak stress compared to native pSFT, albeit less so than GAG-depleted specimens. One hypothesis is that the decellularisation process may instigate a change in the three-dimensional architectural network of endotenon through a rearrangement of collagen-GAG interactions. Further, the reagents used for decellularising pSFT could affect the peritenon, a thin layer of connective tissue enveloping the endotenon (Khan et al., 1999; Kannus, 2000; Yang et al., 2013; Thorpe et al., 2015). An alteration to collagen and elastic fibrils of which it is comprised could compromise its ability to resist deformation under compression, perhaps resulting in a reduced compressive peak stress.

Another material property determined from confined compression of pSFT was the permeability, i.e. resistance to fluid flow through the tissue matrix (Mansour, 2003). GAG-depleted pSFT was found to be twice as permeable as native pSFT, signifying increased ease in water exudation with reduced GAG content. This is likely attributed to the water binding function GAGs carry out in tissue ECM, which was previously described. A study involving porcine ligament also reported a significant increase

in transverse permeability post GAG depletion (Henninger et al., 2010). However, data variance was observed in the GAG-depleted group permeability. This could be a consequence of changes in the structural integrity of the tissue post ChABC treatment as mentioned previously, resulting in non-uniform pre-loading outcomes due to this heightened tissue compliance. The permeability of decellularised pSFT cannot be attributed to GAG content, as this was shown to be unaffected by the decellularisation process (Fig. 4). It may also be a consequence of the structural and conformational alterations that follow the removal of cellular material described previously. However, this does not align fully with the increased fluid flow reported in pSFT post-decellularisation previously (Herbert et al., 2015; Edwards et al., 2019), and therefore warrants further investigation. In doing so, decellularised pSFT permeability could prove beneficial in eliciting an advantageous response *in vivo* (Takayama et al., 2015; Shokrani et al., 2022).

There are several limitations in this study. Firstly, specimen preparation for compression testing, relies on a biopsy punch (Nischal et al., 2008), possibly causing microstructural changes or damage to pSFT specimens. The punch was used on frozen samples to minimise risk of damaging sub-tendon structures, facilitating full depth incision through rotatory motion. Similarly, specimen preparation for tensile testing using a scalpel could have caused microstructural damage along the gauge length of pSFT specimens. Trials were performed to assess the precision and repeatability involved in specimen shaping. Nonetheless, the macroscopic mechanical properties under tensile and compressive loads may have been affected (Lee et al., 2017). Secondly, as discussed previously, the structural changes occurring as a consequence of GAG removal post enzymatic treatment may have resulted in a more compliant tissue. This may have led to the GAG-depleted group being susceptible to initial loads during mechanical testing; therefore, the starting point may have not been uniform across specimens. Thirdly, the length of stress relaxation testing may have resulted in gradual yet minimal freezing along the gauge length of specimens. This may have impacted the long-term viscoelastic behaviour and parameters obtained, along with the instances of large variance observed. Finally, inherent inconsistencies in pSFT and inevitable discrepancies attributed to human error during specimen preparation and experimental methods may have influenced the mechanical behaviour particularly of the GAG-depleted group, for reasons discussed previously. More extensive compressive and tensile characterisation could prove useful to better understand the origins of variability in this study.

5. Conclusions

The biomechanical behaviour of native, GAG-depleted and decellularised pSFT in confined compression conditions was obtained for the first time. GAG removal from tendon matrix significantly reduced peak stress and aggregate modulus, suggesting this component may play a key role in compressive load bearing. Tensile properties of GAG-depleted pSFT were similar to native, untreated tendon, perhaps speaking to the minor role this component may have in withstanding tensile loads. However, the extent to which the gross structural changes observed in GAG-depleted tendon may affect its biomechanics should be further investigated. This study showed, for the first time, that decellularisation does not remove GAGs from pSFT matrix during washing stages, and their mechanical function appears unaffected by the process. Finally, the key biomechanical properties of decellularised pSFT were mostly similar to its native counterpart in compression and tension.

Sources of funding

This work was funded by the Engineering and Physical Sciences Research Council (EPSRC) grant [EP/L014823/1] and supported by the EPSRC programme grant: “Optimising knee therapies through improved population stratification and precision of the intervention” [EP/P001076/1]. J. Solis-Cordova holds a scholarship (71066) from the National Council of Science and Technology of Mexico (CONACyT).

CRediT authorship contribution statement

Jacqueline Solis-Cordova: Writing – review & editing, Writing – original draft, Validation, Project administration, Methodology, Investigation, Formal analysis, Data curation, Conceptualization. **Jennifer H. Edwards:** Writing – review & editing, Validation, Supervision. **Hazel L. Fermor:** Validation, Supervision. **Philip Riches:** Writing – review & editing, Software, Methodology, Formal analysis. **Claire L. Brockett:** Writing – review & editing, Visualization, Supervision, Funding acquisition. **Anthony Herbert:** Writing – review & editing, Visualization, Validation, Supervision, Methodology, Funding acquisition, Conceptualization.

Declaration of competing interest

The authors declare that they have no known competing financial interests or personal relationships that could have appeared to influence the work reported in this paper.

Data availability

The data associated with this paper are openly available from the University of Leeds Data Repository (https://doi.org/10.5518/1289). Further data linked to the work can be accessed through the Institute of Medical and Biological Engineering Knee Dataset (https://doi.org/10.5518/826).

Acknowledgements

Andrew Stockdale for their involvement in discussions on design and optimisation of the novel compression testing rig and Nicola Conway for their expertise in biological and histological methods.

References

Abdelgaied, A., Stanley, M., Galfe, M., Berry, H., Ingham, E., Fisher, J., 2015. Comparison of the biomechanical tensile and compressive properties of decellularised and natural porcine meniscus. J. Biomech. 48 (8), 1389–1396.
Baeurle, S.A., Kiselev, M.G., Makarova, E.S., Nogovitsin, E.A., 2009. Effect of the counterion behavior on the frictional–compressive properties of chondroitin sulfate solutions. Polymer 50 (7), 1805–1813.
Bliss, J.P., 2017. Anterior cruciate ligament injury, reconstruction, and the optimization of outcome. Indian J. Orthop. 51 (5), 606–613.
Böl, M., Ehret, A.E., Leichsenring, K., Ernst, M., 2015. Tissue-scale anisotropy and compressibility of tendon in semi-confined compression tests. J. Biomech. 48 (6), 1092–1098.
Busby, G.A., Grant, M.H., Mackay, S.P., Riches, P.E., 2013. Confined compression of collagen hydrogels. J. Biomech. 46 (4), 837–840.
Casale, J., Crane, J.S., 2022. Biochemistry, glycosaminoglycans. StatPearls Publishing [Online]. Available from: https://www.ncbi.nlm.nih.gov/books/NBK544295/#:~:text=In conclusion%2C glycosaminoglycans (GAGs),%2C anticoagulation%2C and wound repair.
Chan, D.D., Cai, L., Butz, K.D., Trippel, S.B., Nauman, E.A., Neu, C.P., 2016. In vivo articular cartilage deformation: noninvasive quantification of intratissue strain during joint contact in the human knee. Sci. Rep. 6, 19220.
Choi, Y.C., Choi, J.S., Kim, B.S., Kim, J.D., Yoon, H.I., Cho, Y.W., 2012. Decellularized extracellular matrix derived from porcine adipose tissue as a xenogeneic biomaterial for tissue engineering. Tissue Eng. C Methods 18 (11), 866–876.
Crapo, P.M., Gilbert, T.W., Badylak, S.F., 2011. An overview of tissue and whole organ decellularization processes. Biomaterials 32 (12), 3233–3243.
Docking, S., Samiric, T., Scase, E., Purdam, C., Cook, J., 2013. Relationship between compressive loading and ECM changes in tendons. Muscles, ligaments and tendons journal 3 (1), 7–11.
Edwards, J.H., Herbert, A., Jones, G.L., Manfield, I.W., Fisher, J., Ingham, E., 2017. The effects of irradiation on the biological and biomechanical properties of an acellular porcine superflexor tendon graft for cruciate ligament repair. J. Biomed. Mater. Res. B Appl. Biomater. 105 (8), 2477–2486.
Edwards, J.H., Ingham, E., Herbert, A., 2019. Decellularisation affects the strain rate dependent and dynamic mechanical properties of a xenogeneic tendon intended for anterior cruciate ligament replacement. J. Mech. Behav. Biomed. Mater. 91, 18–23.
Edwards, J.H., Jones, G.L., Herbert, A., Fisher, J., Ingham, E., 2021. Integration and functional performance of a decellularised porcine superflexor tendon graft in an ovine model of anterior cruciate ligament reconstruction. Biomaterials 279, 121204.

Ernst, S., Langer, R., Cooney, C.L., Sasisekharan, R., 1995. Enzymatic degradation of glycosaminoglycans. Crit. Rev. Biochem. Mol. Biol. 30 (5), 387–444.
Fang, F., Lake, S.P., 2015. Multiscale strain analysis of tendon subjected to shear and compression demonstrates strain attenuation, fiber sliding, and reorganization. J. Orthop. Res. 33 (11), 1704–1712.
Fang, F., Sawhney, A.S., Lake, S.P., 2014. Different regions of bovine deep digital flexor tendon exhibit distinct elastic, but not viscous, mechanical properties under both compression and shear loading. J. Biomech. 47 (12), 2869–2877.
Feitosa, V.L.C., Reis, F.P., Esquisatto, M.A.M., Joazeiro, P.P., Vidal, B.C., Pimentel, E.R., 2006. Comparative ultrastructural analysis of different regions of two digital flexor tendons of pigs. Micron 37 (6), 518–525.
Fermor, H.L., Russell, S.L., Williams, S., Fisher, J., Ingham, E., 2015. Development and characterisation of a decellularised bovine osteochondral biomaterial for cartilage repair. J. Mater. Sci. Mater. Med. 26 (5), 186.
Fessel, G., Snedeker, J.G., 2011. Equivalent stiffness after glycosaminoglycan depletion in tendon — an ultra-structural finite element model and corresponding experiments. J. Theor. Biol. 268 (1), 77–83.
Fishman, J.M., Lowdell, M.W., Urbani, L., Ansari, T., Burns, A.J., Turmaine, M., North, J., Sibbons, P., Seifalian, A.M., Wood, K.J., Birchall, M.A., De Coppi, P., 2013. Immunomodulatory effect of a decellularized skeletal muscle scaffold in a discordant xenotransplantation model. Proc. Natl. Acad. Sci. USA 110 (35), 14360–14365.
Gans, I., Retzky, J.S., Jones, L.C., Tanaka, M.J., 2018. Epidemiology of recurrent anterior cruciate ligament injuries in national collegiate athletic association sports: the injury surveillance program, 2004-2014 Orthopaedic J. Sports Med. 6 (6), 2325967118777823.
Gautieri, A., Vesentini, S., Redaelli, A., Ballarini, R., 2013. Modeling and measuring visco-elastic properties: from collagen molecules to collagen fibrils. Int. J. Non Lin. Mech. 56, 25–33.
Gilbert, T.W., Sellaro, T.L., Badylak, S.F., 2006. Decellularization of tissues and organs. Biomaterials 27 (19), 3675–3683.
Gilpin, A., Yang, Y., 2017. Decellularization strategies for regenerative medicine: from processing techniques to applications. BioMed Res. Int.
Harvey, A., Thomas, N.P., Amis, A.A., 2005. Fixation of the graft in reconstruction of the anterior cruciate ligament. J. Bone Joint Surg. Br. 87-B (5), 593–603.
Henninger, H.B., Underwood, C.J., Ateshian, G.A., Weiss, J.A., 2010. Effect of sulfated glycosaminoglycan digestion on the transverse permeability of medial collateral ligament. J. Biomech. 43 (13), 2567–2573.
Herbert, A., Brown, C., Rooney, P., Kearney, J., Ingham, E., Fisher, J., 2016. Bi-linear mechanical property determination of acellular human patellar tendon grafts for use in anterior cruciate ligament replacement. J. Biomech.
Herbert, A., Edwards, J.H., Jones, G.L., Ingham, E., Fisher, J., 2017. The effects of irradiation dose and storage time following treatment on the viscoelastic properties of decellularised porcine super flexor tendon. J. Biomech. 57, 157–160.
Herbert, A., Jones, G.L., Ingham, E., Fisher, J., 2015. A biomechanical characterisation of acellular porcine super flexor tendons for use in anterior cruciate ligament replacement: investigation into the effects of fat reduction and bioburden reduction bioprocesses. J. Biomech. 48 (1), 22–29.
Jamil, T., Ansari, U., Najabat Ali, M., Mir, M., 2017. A review on biomechanical and treatment aspects associated with anterior cruciate ligament. Irbm 38 (1), 13–25.
Janssen, R.P.A., Scheffler, S.U., 2014. Intra-articular remodelling of hamstring tendon grafts after anterior cruciate ligament reconstruction. Knee Surg. Sports Traumatol. Arthrosc. : official journal of the ESSKA 22 (9), 2102–2108.
Jimenez Rios, J.L., Steif, P.S., Rabin, Y., 2007. Stress-strain measurements and viscoelastic response of blood vessels cryopreserved by vitrification. Ann. Biomed. Eng. 35 (12), 2077–2086.
Jones, G.L., Herbert, A., Berry, H., Edwards, J.H., Fisher, J., Ingham, E., 2017. Decellularization and characterization of porcine superflexor tendon: a potential anterior cruciate ligament replacement. Tissue Eng. 23 (3–4), 124–134.
Kannus, P., 2000. Structure of the tendon connective tissue. Scand. J. Med. Sci. Sports 10 (6), 312–320.
Khan, K.M., Cook, J.L., Bonar, F., Harcourt, P., Astrom, M., 1999. Histopathology of common tendinopathies. Update and implications for clinical management. Sports Med. 27 (6), 393–408.
Kim, Y.S., Majid, M., Melchiorri, A.J., Mikos, A.G., 2019. Applications of decellularized extracellular matrix in bone and cartilage tissue engineering. Bioeng. Transl. Med.
Koob, T.J., Clark, P.E., Hernandez, D.J., Thurmond, F.A., Vogel, K.G., 1992. Compression loading in vitro regulates proteoglycan synthesis by tendon fibrocartilage. Arch. Biochem. Biophys. 298 (1), 303–312.
Lee, A.H., Szczesny, S.E., Santare, M.H., Elliott, D.M., 2017. Investigating mechanisms of tendon damage by measuring multi-scale recovery following tensile loading. Acta Biomater. 57, 363–372.
Lee, S.-B., Nakajima, T., Luo, Z.-P., Zobitz, M.E., Chang, Y.-W., An, K.-N., 2000. The bursal and articular sides of the supraspinatus tendon have a different compressive stiffness. Clin. BioMech. 15 (4), 241–247.
Lujan, T.J., Underwood, C.J., Henninger, H.B., Thompson, B.M., Weiss, J.A., 2007. Effect of dermatan sulfate glycosaminoglycans on the quasi-static material properties of the human medial collateral ligament. J. Orthop. Res. 25 (7), 894–903.
Lujan, T.J., Underwood, C.J., Jacobs, N.T., Weiss, J.A., 2009. Contribution of glycosaminoglycans to viscoelastic tensile behavior of human ligament. J. Appl. Physiol. 106 (2), 423–431. Bethesda, Md: 1985.
Maas, S.A., Ellis, B.J., Ateshian, G.A., Weiss, J.A., 2012. FEBio: finite elements for biomechanics. J. Biomech. Eng. 134 (1), 11005.
Macaulay, A.A., Perfetti, D.C., Levine, W.N., 2012. Anterior cruciate ligament graft choices. Sports health 4 (1), 63–68.
Mansour, J.M., 2003. Biomechanics of Cartilage *in: Kinesiology: the Mechanics And Pathomechanics Of Human Movement*, pp. 69–83.
Nischal, U., Kc, N., Khopkar, U., 2008. Techniques of skin biopsy and practical considerations. J. Cutan. Aesthetic Surg. 1 (2), 107–111.
Rahouadj, R., De Isla, N., Laurent, C., Liu, X., Wang, X., 2018. Defining a scaffold for ligament tissue engineering: what has been done, and what still needs to be done. J. Cell. Immunother. 4 (1), 4–9.
Rigozzi, S., Müller, R., Stemmer, A., Snedeker, J.G., 2013. Tendon glycosaminoglycan proteoglycan sidechains promote collagen fibril sliding—AFM observations at the nanoscale. J. Biomech. 46 (4), 813–818.
Ryan, C.N.M., Sorushanova, A., Lomas, A.J., Mullen, A.M., Pandit, A., Zeugolis, D.I., 2015. Glycosaminoglycans in tendon physiology, pathophysiology, and therapy. Bioconjugate Chem. 26 (7), 1237–1251.
Sackett, S.D., Tremmel, D.M., Ma, F., Feeney, A.K., Maguire, R.M., Brown, M.E., Zhou, Y., Li, X., O'Brien, C., Li, L., Burlingham, W.J., Odorico, J.S., 2018. Extracellular matrix scaffold and hydrogel derived from decellularized and delipidized human pancreas. Sci. Rep. 8 (1), 10452.
Screen, H.R.C., 2008. Investigating load relaxation mechanics in tendon. J. Mech. Behav. Biomed. Mater. 1 (1), 51–58.
Screen, H.R.C., Chhaya, V.H., Greenwald, S.E., Bader, D.L., Lee, D.A., Shelton, J.C., 2006. The influence of swelling and matrix degradation on the microstructural integrity of tendon. Acta Biomater. 2 (5), 505–513.
Screen, H.R.C., Shelton, J.C., Chhaya, V.H., Kayser, M.V., Bader, D.L., Lee, D.A., 2005. The influence of noncollagenous matrix components on the micromechanical environment of tendon fascicles. Ann. Biomed. Eng. 33 (8), 1090–1099.
Shadwick, R.E., 1990. Elastic energy storage in tendons: mechanical differences related to function and age. J. Appl. Physiol. 68 (3), 1033–1040.
Shi, D., Sheng, A., Chi, L., 2021. Glycosaminoglycan-protein interactions and their roles in human disease. Front. Mol. Biosci. 8, 639666.
Shokrani, H., Shokrani, A., Sajadi, S.M., Seidi, F., Mashhadzadeh, A.H., Rabiee, N., Saeb, M.R., Aminabhavi, T., Webster, T.J., 2022. Cell-seeded biomaterial scaffolds: the urgent need for unanswered accelerated angiogenesis. Int. J. Nanomed. 17, 1035–1068.
Speziali, A., Delcogliano, M., Tei, M., Placella, G., Bartoli, M., Menghi, A., Cerulli, G., 2014. Fixation techniques for the anterior cruciate ligament reconstruction: early follow-up. A systematic review of level I and II therapeutic studies. MUSCULOSKELETAL SURGERY 98 (3), 179–187.
Stapleton, T.W., Ingram, J., Katta, J., Knight, R., Korossis, S., Fisher, J., Ingham, E., 2008. Development and characterization of an acellular porcine medial meniscus for use in tissue engineering. Tissue Eng. 14 (4), 505–518. Part A.
Svensson, R.B., Hassenkam, T., Hansen, P., Kjaer, M., Magnusson, S.P., 2011. Tensile force transmission in human patellar tendon fascicles is not mediated by glycosaminoglycans. Connect. Tissue Res. 52 (5), 415–421.
Takayama, K., Kawakami, Y., Mifune, Y., Matsumoto, T., Tang, Y., Cummins, J.H., Greco, N., Kuroda, R., Kurosaka, M., Wang, B., Fu, F.H., Huard, J., 2015. The effect of blocking angiogenesis on anterior cruciate ligament healing following stem cell transplantation. Biomaterials 60, 9–19.
Thorpe, C.T., Birch, H.L., Clegg, P.D., Screen, H.R.C., 2015. Tendon physiology and mechanical behavior: structure–function relationships [Online]. In: Gomes, M.E., Reis, R.L., Rodrigues, M.T. (Eds.), Tendon Regeneration. Academic Press, Boston, pp. 3–39. Available from: http://www.sciencedirect.com/science/article/pii/B9780128015902000016.
Viidik, A., 1966. Biomechanics and Functional Adaption of Tendons and Joint Ligaments. *Studies On the Anatomy And Function Of Bone And Joints*, pp. 17–39.
Villa Albers, M.B., Guenther, D., van Eck, C.F., Fu, F.H., 2017. Individualized anatomical anterior cruciate ligament reconstruction. Operat. Tech. Orthop. 27 (1), 20–26.
Vogel, K.G., Koob, T.J., 1989. Structural specialization in tendons under compression. In: Jeon, K.W., Friedlander, M. (Eds.), International Review of Cytology. Academic Press, pp. 267–293. Available from: https://www.sciencedirect.com/science/article/pii/S0074769608606324.
Vyas, D., Rabuck, S.J., Harner, C.D., 2012. Allograft anterior cruciate ligament reconstruction: indications, Techniques, and outcomes. J. Orthop. Sports Phys. Ther.
Whitaker, S., Edwards, J.H., Guy, S., Ingham, E., Herbert, A., 2019. Stratifying the mechanical performance of a decellularized xenogeneic tendon graft for anterior cruciate ligament reconstruction as a function of graft diameter. Bone & joint research 8 (11), 518–525.
Wight, T.N., Kinsella, M.G., Qwarnström, E.E., 1992. The role of proteoglycans in cell adhesion, migration and proliferation. Curr. Opin. Cell Biol. 4 (5), 793–801.
Williams, L.N., Elder, S.H., Bouvard, J.L., Horstemeyer, M.F., 2008. The anisotropic compressive mechanical properties of the rabbit patellar tendon. Biorheology 45 (5), 577–586.
Wilmink, J., Wilson, A.M., Goodship, A.E., 1992. Functional significance of the morphology and micromechanics of collagen fibres in relation to partial rupture of the superficial digital flexor tendon in racehorses. Res. Vet. Sci. 53 (3), 354–359.
Woods, T., Gratzer, P.F., 2005. Effectiveness of three extraction techniques in the development of a decellularized bone–anterior cruciate ligament–bone graft. Biomaterials 26 (35), 7339–7349.
Yang, G., Rothrauff, B.B., Tuan, R.S., 2013. Tendon and ligament regeneration and repair: clinical relevance and developmental paradigm. Birth Defects Res., Part C 99 (3), 203–222.